Rapid Communications   Editors' Suggestion

Environmentally sensitive theory of electronic and optical transitions in atomically thin semiconductors

Yeongsu Cho and Timothy C. Berkelbach[*]

Department of Chemistry and James Franck Institute, University of Chicago, Chicago, Illinois 60637, USA

We present an electrostatic theory of band-gap renormalization in atomically thin semiconductors that captures the strong sensitivity to the surrounding dielectric environment. In particular, our theory aims to correct known band gaps, such as that of the three-dimensional bulk crystal. Combining our quasiparticle band gaps with an effective-mass theory of excitons yields environmentally sensitive optical gaps as would be observed in absorption or photoluminescence. For an isolated monolayer of MoS_2, the presented theory is in good agreement with *ab initio* results based on the *GW* approximation and the Bethe-Salpeter equation. We find that changes in the electronic band gap are almost exactly offset by changes in the exciton binding energy such that the energy of the first optical transition is nearly independent of the electrostatic environment, rationalizing experimental observations.

Introduction. Atomically thin materials exhibit remarkable electronic properties due to their quasi-two-dimensional nature [1–4]. However, their size also makes them extremely sensitive to their local environment. A complete theoretical picture must simultaneously treat the two-dimensional nature of carriers and the dielectric character of the surroundings. This latter property is the primary distinction between atomically thin materials [such as the transition-metal dichalcogenides (TMDCs)] and heterostructured semiconductor quantum wells (such as GaAs in AlGaAs).

To date, many theoretical studies of atomically thin materials have focused on the excitonic properties, including the large exciton binding energy [5–7], the unique excitonic Rydberg series [8,9], the nature of selection rules [10–12], and Berry phase modifications of the exciton spectrum [13,14]. Surprisingly, the quasiparticle band gap has received significantly less attention, especially from simplified microscopic theories, perhaps because it is challenging to measure experimentally. In fact, simple theories of the exciton binding energy are often times used in conjunction with the experimentally measured optical gap in order to estimate the quasiparticle band gap [8,15].

The *GW* approximation represents the current method of choice for the accurate calculation of band structures and band gaps [16,17]. However, the quasi-two-dimensional nature of the atomically thin materials makes these calculations very challenging to converge [18–20]. In this Rapid Communication, we provide a simple electrostatic theory of band-gap renormalization due to electrostatic proximity effects. Through combination with an effective-mass theory of the exciton binding energy, we find that the optical gap—i.e. the sum of the band gap and the (negative) exciton binding energy— is extremely insensitive to the dielectric environment. This represents a quasianalytical demonstration of this remarkable effect.

The band gap of nanoscale materials differs from that of the three-dimensional bulk parent material because of two separate effects: carrier confinement and dielectric contrast. In the first case, the geometric confinement of carriers leads to an increased kinetic energy and a concomitantly larger band gap. However, in layered materials (such as the TMDCs), the two-dimensional confinement is already largely reflected in the bulk band gap as evidenced by the small bandwidth in the perpendicular (stacking) direction. Therefore, in the following, we employ this idealized scenario of carriers confined to two dimensions, even when describing the bulk material. In particular, this approximation is invoked to describe low-energy carriers at the K points of the Brillouin zone; here, the wave-function character is primarily that of transition-metal d orbitals, which are confined to the center of the TMDC layer, precluding strong interlayer hybridization. In Fig. 1, we show the band structure of bulk and monolayer MoS_2 calculated using density functional theory (DFT) [21]. The monolayer band gap at the K point is only 0.09 eV larger than that of the bulk, indicating that any band-gap renormalization due to carrier confinement is already (largely) accounted for in the bulk band gap; we henceforth neglect this small shift so as to focus on alternative effects while treating the monolayer and bulk on equal footing. We emphasize that this geometric carrier confinement is a one-electron (kinetic-energy) effect that is well described by density functional theory—unlike dielectric screening effects.

As mentioned above, a second source of band-gap renormalization in nanomaterials is the dielectric contrast effect. Physically, we recall that the quasiparticle conduction and valence bands measure the electron affinities and ionization potentials, respectively. The excess charge created in these processes polarizes the material and its environment such that the potential energy of the charge depends on the local dielectric geometry. We model atomically thin semiconductors as a slab of dielectric constant ε_1 and width d, surrounded by environmental dielectric constants ε_2 below and ε_3 above
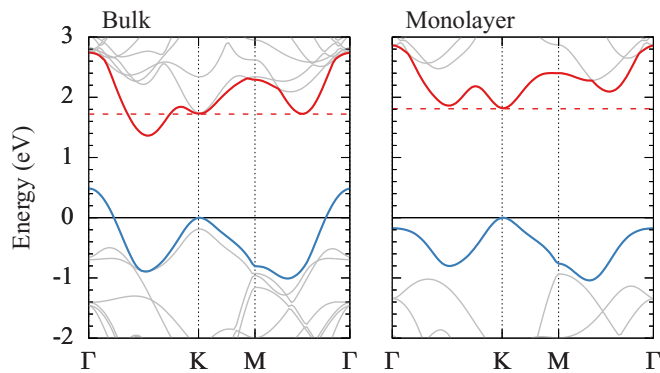
*berkelbach@uchicago.edu

FIG. 1. Band structures of bulk and monolayer MoS_2 calculated with density functional theory. The direct band gap (at the K point) is 0.09 eV larger for the monolayer than for the bulk due to the carrier confinement effect.

as shown in Fig. 2. Consistent with the arguments presented above, the carriers will be assumed to occupy the center of the slab at $z = 0$.

We now proceed to calculate the band-structure corrections due to such a heterogeneous dielectric environment. We assume that a *reference* many-body band gap is known; here, we will primarily consider band-structure corrections to the three-dimensional bulk material. The three-dimensional bulk band gap is the simplest reference value because it can easily be obtained from calculation or experiment, owing to the relatively strong screening and small exciton binding energy of three-dimensional bulk semiconductors. Although our theory could also be applied to correct the band gap of an isolated monolayer due to changes in its dielectric environment, we emphasize that the latter reference band gap is much harder to calculate or extract from experiment.

Corrections to the three-dimensional bulk band gap will be calculated in two ways: (1) classically, using electrostatic continuum theory; and (2) quantum mechanically, using the static Coulomb-hole plus screened exchange (COHSEX) approximation to the quantum-mechanical GW self-energy. When correcting a reference band structure, we require the *difference* in the screened Coulomb interaction $\delta W(\boldsymbol{r}, \boldsymbol{r}') \equiv W(\boldsymbol{r}, \boldsymbol{r}') - W^{\mathrm{ref}}(\boldsymbol{r}, \boldsymbol{r}')$, where W is the total screened Coulomb interaction. We calculate the respective screened interactions through their electrostatic counterparts associated with the slab dielectric geometry shown in Fig. 2. Although this is a classical approximation, which neglects local field effects, it avoids the high cost of an *ab initio* calculation of the screened Coulomb interaction.
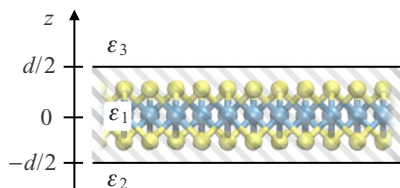

FIG. 2. Idealized dielectric slab geometry used to model the electrostatics of atomically thin semiconductors.

In recent years, effective-mass theories of atomically thin materials have made frequent use of the model potential energy derived by Rytova [22] and Keldysh [23] (RK),

$$W^{\mathrm{RK}}(\rho) = \frac{\pi e^2}{(\varepsilon_2 + \varepsilon_3)\rho_0} \left[H_0\left(\frac{\rho}{\rho_0}\right) - Y_0\left(\frac{\rho}{\rho_0}\right) \right], \quad (1)$$

where H_0 and Y_0 are the Struve function and the Bessel function of the second kind and ρ is the two-dimensional in-plane separation. The screening length is given by $\rho_0 = \varepsilon_1 d/(\varepsilon_2 + \varepsilon_3)$ and can be related to a two-dimensional sheet polarizability [5,24]. For the purposes of the present Rapid Communication, the RK potential suffers from two deficiencies. First, it applies only in the limit of extreme dielectric mismatch between the slab and its surroundings; although this approximation is good for isolated (suspended) monolayers, it breaks down in more general dielectric environments. Second, the RK potential has an unphysical logarithmic divergence at $\rho = 0$, which precludes its use in simple electrostatic theories of band-gap renormalization. Instead, we employ the exact solution of the finite-thickness electrostatic problem shown in Fig. 2. We emphasize that the logarithmic behavior of the RK potential is correct over some intermediate length scale and only incorrect for $\rho \lesssim d$.

The potential energy of two charges in a slab with locations z_1, z_2, and in-plane separation ρ can be calculated via image charges to give a screened interaction $W(z_1, z_2, \rho)$ [25]. In the center of the slab ($z_1 = z_2 = 0$), we find

$$W(\rho) = \frac{e^2}{\varepsilon_1 \rho} + 2 \sum_{n=1}^{\infty} \frac{e^2 L_{12}^n L_{13}^n}{\varepsilon_1 \{\rho^2 + (2nd)^2\}^{1/2}}$$
$$+ (L_{12} + L_{13}) \sum_{n=0}^{\infty} \frac{e^2 L_{12}^n L_{13}^n}{\varepsilon_1 \{\rho^2 + [(2n+1)d]^2\}^{1/2}}, \quad (2)$$

where $L_{1n} = (\varepsilon_1 - \varepsilon_n)/(\varepsilon_1 + \varepsilon_n)$. Unlike the RK potential, this continuum electrostatic potential is correct in the uniform case of $\varepsilon_1 = \varepsilon_2 = \varepsilon_3$ and has the proper divergence as $\rho \to 0$. Atomistically, the dielectric function should go to unity at $q \to \infty$ (i.e., on subatomic length scales). Instead of the coarse-grained electrostatic theories employed here, all of our calculations could easily be performed with an *ab initio* screened Coulomb interaction as could be efficiently obtained using the recently introduced quantum electrostatic heterostructure technique [26,27].

Electrostatic solution. In the simplest electrostatic (Born) approximation, the conduction- and valence-band corrections in the center of the slab are given by the self-interaction energy [25,28],

$$\delta \Sigma_{\mathrm{c/v}} = \pm \frac{1}{2} \lim_{\rho \to 0} \delta W(\rho), \quad (3)$$

which is nondivergent due to the use of an interaction difference δW as long as the slab dielectric ε_1 is identical in both W and W^{ref}. When the reference potential energy is that of a uniform bulk dielectric, i.e., $W^{\mathrm{ref}}(\boldsymbol{r}, \boldsymbol{r}') = e^2/(\varepsilon_1 |\boldsymbol{r} - \boldsymbol{r}'|)$, then the electrostatic corrections using Eqs. (2) and (3) can be

summed analytically to give the relatively simple expression,

$$\delta\Sigma_{c/v} = \pm\frac{e^2}{2\varepsilon_1 d}\left\{\frac{(L_{12}+L_{13})}{\sqrt{L_{12}L_{13}}}\tanh^{-1}(\sqrt{L_{12}L_{13}})\right.$$
$$\left. - \ln(1-L_{12}L_{13})\right\}, \tag{4}$$

where we used $\ln(1-x) = -\sum_{n=1}^{\infty} x^n/n$ and $\tanh^{-1}(x) = \sum_{n=0}^{\infty} x^{2n+1}/(2n+1)$.

Tight-binding COHSEX. First-principles band-structure calculations typically employ the GW approximation to the self-energy. In the static screening limit, this approximation yields two contributions to the self-energy: a Coulomb-hole (COH) term and a screened exchange (SEX) term [16]. By assuming that an initial many-body *reference* band structure is known, we can calculate corrections in alternative electrostatic environments as diagonal elements of the self-energy operator, which leads to

$$\delta\Sigma_p^{\text{COH}}(\boldsymbol{k}) = \frac{1}{2}\lim_{\rho\to 0}\delta W(\rho), \tag{5a}$$

$$\delta\Sigma_p^{\text{SEX}}(\boldsymbol{k}) = -\frac{1}{N_k}\int d^2\boldsymbol{x}_1 \int d^2\boldsymbol{x}_2 \phi_{p,\boldsymbol{k}}^*(\boldsymbol{x}_1)\rho(\boldsymbol{x}_1,\boldsymbol{x}_2)$$
$$\times \delta W(\rho)\phi_{p,\boldsymbol{k}}(\boldsymbol{x}_2), \tag{5b}$$

where $\boldsymbol{x} = (\boldsymbol{\rho},\tau)$ is the combined space and spin variable, $\rho(\boldsymbol{x}_1,\boldsymbol{x}_2)$ is the reduced density matrix of the mean-field reference, N_k is the number of k points sampled in the Brillouin zone, and $p = (\text{c,v})$ indexes the conduction or valence band. In the simplest approximation, we consider the two-band tight-binding Hamiltonian [29],

$$H(\boldsymbol{k}) = \begin{pmatrix} E_{\text{g}}/2 & at(k_x+ik_y) \\ at(k_x-ik_y) & -E_{\text{g}}/2 \end{pmatrix}, \tag{6}$$

with eigenvectors $\langle\boldsymbol{x}|p\boldsymbol{k}\rangle = \phi_{p\boldsymbol{k}}(\boldsymbol{x})$ and eigenvalues $E_{\text{c/v}}(\boldsymbol{k}) = \pm\frac{1}{2}\sqrt{E_g^2 + (2atk)^2}$. In this Hamiltonian, E_{g} is the band gap, a is the lattice constant, and t is the interatomic transfer integral. A single (doubly occupied) valence band leads to the simple density-matrix $\rho(\boldsymbol{x}_1,\boldsymbol{x}_2) = \sum_{\boldsymbol{q}}\phi_{v\boldsymbol{q}}(\boldsymbol{x}_1)\phi_{v\boldsymbol{q}}^*(\boldsymbol{x}_2)$. Further simplifications concerning the locality of the underlying real-space basis functions leads to the SEX self-energy,

$$\delta\Sigma_p^{\text{SEX}}(\boldsymbol{k}) = -\frac{1}{N_k}\sum_{\boldsymbol{q}}|\langle p\boldsymbol{k}|v\boldsymbol{q}\rangle|^2 {\sum_{\boldsymbol{G}}}' \delta W(\boldsymbol{G}+\boldsymbol{q}-\boldsymbol{k}), \tag{7}$$

where

$$\delta W(\boldsymbol{k}) = \frac{1}{A_{\text{BZ}}}\int d^2\rho\, e^{i\boldsymbol{\rho}\cdot\boldsymbol{k}}\delta W(\rho), \tag{8}$$

A_{BZ} is the area of the Brillouin zone and the primed summation in Eq. (7) excludes the term with $\boldsymbol{G} = 0$ when $\boldsymbol{k} = \boldsymbol{q}$. Summarizing, the COH term yields a positive constant shift to both the conduction and the valence bands, which is *exactly* equal to the (positive) correction obtained in the pure electrostatic theory presented above; the SEX term yields a negative k-dependent shift with a magnitude that depends on overlap

factors between the valence band and the band being corrected. To a reasonable approximation (verified numerically below), the SEX contribution is negligible in the conduction band (due to vanishing overlaps) but is substantial in the valence band. Furthermore, if the squared overlap is approximated by unity, i.e., $|\langle v\boldsymbol{k}|v\boldsymbol{q}\rangle|^2 \approx 1$, then the magnitude of the SEX correction in the valence band is exactly twice that of the COH term. As shown in Ref. [30] for the case of molecules near metal surfaces, we therefore have simple approximate COHSEX corrections given by $\delta\Sigma_{\text{c}} \approx +P - 0 = +P$ and $\delta\Sigma_{\text{v}} \approx +P - 2P = -P$, where $P = \frac{1}{2}\lim_{\rho\to 0}\delta W(\rho)$ is precisely the electrostatically derived correction. In reality, the squared overlap can be less than one, and the SEX correction to the valence band (and thus the band gap) will be slightly smaller than that of the continuum electrostatic theory.

Effective-mass theory of excitons. The optical gap as measured in linear spectroscopies, such as absorption or photoluminescence, is the sum of the quasiparticle band gap and the (negative) exciton binding energy. At a similar level of theory to that used so far, the exciton states can be calculated using an effective-mass theory,

$$\left[-\frac{1}{2\mu}\nabla_{\boldsymbol{\rho}}^2 - W(\rho)\right]\Psi_n(\boldsymbol{\rho}) = E_n\Psi_n(\boldsymbol{\rho}), \tag{9}$$

where ρ is the electron-hole separation, Ψ_n is the exciton wave function, and E_n is its binding energy. The material parameters enter through the exciton-reduced mass $\mu = m_{\text{e}}m_{\text{h}}/(m_{\text{e}}+m_{\text{h}})$ and the same screened Coulomb interaction W as used above. Due to the angular symmetry, the effective-mass equation is a simple one-dimensional Schrödinger equation in the radial direction, which may be solved numerically exactly on a real-space grid to obtain the full Rydberg series of band-edge excitons. The exciton wave functions and binding energies are sensitive to the local dielectric environment where higher dielectric constants result in stronger screening, more diffuse wave functions, and smaller binding energies.

Results. Although our theory is appropriate for any atomically thin semiconductor, we will apply it to the well-studied case of MoS_2, a prototypical layered transition-metal dichalcogenide. As is common for quantum-confined materials, we correct the bulk band gap using a uniform reference Coulomb potential with $\varepsilon_1 = \varepsilon_2 = \varepsilon_3$, i.e., $W^{\text{ref}}(\boldsymbol{r},\boldsymbol{r}') = e^2/(\varepsilon_1|\boldsymbol{r}-\boldsymbol{r}'|)$ [31]; for MoS_2, we use $\varepsilon_1 = 14$, which is approximately the value of the in-plane element of the bulk dielectric tensor, calculated using various first-principles techniques including density functional theory and the GW approximation [5]. For the monolayer, we solve the electrostatic problem in Fig. 2 with $\varepsilon_1 = 14$ and $d = 6$ Å, which roughly corresponds to the perpendicular extent of monolayer MoS_2; these parameters yield the ideal screening length $\rho_0 = 42$ Å in good agreement with the *ab initio* value of 41.5 Å [5]. We take the reference A-series band gap of bulk MoS_2 to be $E_{\text{g}}^{\text{bulk}} = 1.98$ eV [32], and for the tight-binding Hamiltonian in Eq. (6), we use $at = 3.51$ eV Å [29]. For the exciton problem in Eq. (9), we use the effective-mass $\mu = 0.25m_0$ as parametrized by DFT calculations [5].

First, we consider the experimentally relevant situation of a monolayer on a substrate with dielectric constant ε_2 and vacuum above ($\varepsilon_3 = 1$). In Fig. 3(a), we show the band gap
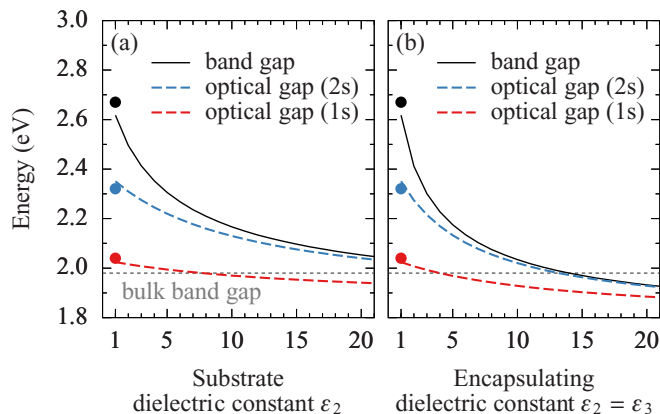
FIG. 3. The quasiparticle band gap and optical gap (i.e., excitonic transition energy) of monolayer MoS_2 as a function of (a) the substrate dielectric constant with vacuum above ($\varepsilon_3 = 1$) and (b) the encapsulating dielectric constant ($\varepsilon_2 = \varepsilon_3$). The bulk band gap, which is a fixed parameter in the theory, is indicated by a dotted gray line. The filled circles at $\varepsilon_2 = 1$ indicate the *ab initio* G_0W_0 result (the black circle) and the Bethe-Salpeter equation results (the red and blue circles) for an isolated monolayer from Ref. [20].

calculated using the tight-binding COHSEX approximation as a function of the substrate dielectric constant. The purely electrostatic approximation in Eq. (4) is not shown but gives nearly identical results, predicting band gaps that are slightly larger (about 0.05 eV), which can be understood based on the arguments presented above. Remarkably, the simple theory presented here—parametrized only on bulk data and an estimate of the monolayer width—predicts an isolated monolayer ($\varepsilon_2 = 1$) band gap of 2.62 eV (a 0.64-eV increase from bulk); this compares very favorably to a recent carefully converged *ab initio* calculation using the many-body G_0W_0 approximation, which predicts 2.67 eV [20]. This huge increase in the quasiparticle band gap reflects the strong role played by reduced dielectric screening in atomically thin materials.

At larger values of ε_2, the increased screening ability of the substrate yields a rapid decrease in the band gap, demonstrating the strong sensitivity of atomically thin materials to their local environment. Even a modest substrate, such as silica, with a dielectric constant of $\varepsilon_2 \approx 4$, is predicted to have a band gap of 2.35 eV, which is 0.27 eV smaller than an ideal suspended monolayer. On graphite, with $\varepsilon_2 \approx 10$, the band gap is reduced by 0.45 eV. Similar results have been obtained with an approximate treatment of substrate screening in otherwise *ab initio* G_0W_0 calculations [33,34]. These findings underscore the care required when comparing experimental measurements on substrates to *ab initio* calculations of isolated atomically thin materials. In reverse, the simple formula given in Eq. (4) can be used to infer the ideal suspended band gap based on measurements performed on substrates.

In Fig. 3(a), we also show the optical gap for the 1s and 2s exciton states, obtained by summing the quasiparticle band gap and the exciton binding energies of each state as a function of the substrate dielectric constant. For the isolated monolayer, we predict optical gaps of 2.03 and 2.35 eV (positive binding energies of 0.59 and 0.27 eV) for the 1s and 2s states, respectively. Again, these compare well with converged *ab*

initio calculations using the Bethe-Salpeter equation, which predict optical gaps of 2.04 and 2.32 eV (binding energies of 0.63 and 0.35 eV) [20].

As the dielectric constant of the substrate increases, the exciton binding energies are reduced due to increased environmental screening. Remarkably, the competing effects in the band gap and 1s binding energy almost exactly cancel. Up to a substrate dielectric constant of $\varepsilon_2 = 20$, the 1s optical transition energy only changes by 0.1 eV. In the aforementioned examples of silica and graphite substrates, the exciton binding energy is reduced by 0.24 and 0.49 eV, respectively. Not only is the optical transition energy roughly constant, but the cancellation is almost perfect such that the monolayer transition energy is nearly identical to the bulk transition energy (the bulk band gap and optical gap roughly coincide because the exciton binding energy is only about 0.04 eV [32]).

In addition to the well-known observation that the optical gap of bulk TMDCs is almost identical to that of monolayers, the effects predicted by the theory are in good agreement with a number of other more detailed experimental findings, such as the insensitivity of the optical gap in TMDCs when comparing suspended samples and samples on fused-silica substrates [35]. Identical effects in the band gap, optical gap, and exciton binding energy have been observed in a joint experimental-computational study of $MoSe_2$ on bilayer graphene and graphite: The latter exhibits a 0.24-eV reduction in the band gap and a concomitant 0.28-eV reduction in the exciton binding energy, leading to a minimal change in the optical gap [33]. Similar competing effects have been observed in the optical properties of doped or photoexcited TMDCs [36], although the screening physics is quite different.

The above analysis can be repeated for more general dielectric environments; the results of uniform encapsulation ($\varepsilon_2 = \varepsilon_3$) are shown in Fig. 3(b). Although the qualitative behavior is the same, the effects are naturally stronger due to the simultaneous screening from above and below the monolayer.

Finally, we mention that, although we have focused on the band gap, our theory separately predicts changes to the ionization potential and electron affinity. The environmental renormalization of these quantities may be of interest for photochemistry, catalysis, or device engineering.

Conclusions. To summarize, we have presented a simple but powerful theory of environmentally sensitive electronic and optical transition energies in atomically thin materials. Although the theory shows that the quasiparticle band gap and the exciton binding energy are individually very sensitive to their local dielectric environment, the sum of the two (the lowest-energy optical transition) is almost completely insensitive. In some sense, this is an unfortunate state of affairs for the use of atomically thin materials as environmental or chemical sensors because optical transitions are the simplest to measure (by absorption or photoluminescence); by contrast, measuring the band gap by photoemission or electron tunneling experiments is much more difficult. Nonetheless, the theory presented here enables rapid and quantitative exploration of accessible energetic changes through dielectric engineering.

In light of our results, we propose that the higher-lying excitonic resonances are promising optical reporters of the local environment. Even the 2s resonance—which can typically be resolved in experiments—is predicted to redshift

by 0.1 eV when a suspended sample is placed on a silica substrate. Indeed, the $1s$-$2s$ separation was used recently as an experimental probe of environmental effects [15].

Going forward, this approach can be used to study other environmentally sensitive atomically thin materials, such as black phosphorous [37]. These techniques can also be applied to more heterogeneous dielectric environments as might be experimentally realized through patterning [15], molecu-

lar coverage [38,39], or functional layered heterostructures [40–42]. In many cases, explicit electronic hybridization and charge transfer should be accounted for in the theory. Work along these lines is currently in progress.

[1] K. F. Mak, M. Y. Sfeir, Y. Wu, C. H. Lui, J. A. Misewich, and T. F. Heinz, Phys. Rev. Lett. **101**, 196405 (2008).

[2] A. H. C. Neto, F. Guinea, N. M. R. Peres, K. S. Novoselov, and A. K. Geim, Rev. Mod. Phys. **81**, 109 (2009).

[3] A. Splendiani, L. Sun, Y. Zhang, T. Li, J. Kim, C.-Y. Chim, G. Galli, and F. Wang, Nano Lett. **10**, 1271 (2010).

[4] K. F. Mak, C. Lee, J. C. Hone, J. Shan, and T. F. Heinz, Phys. Rev. Lett. **105**, 136805 (2010).

[5] T. C. Berkelbach, M. S. Hybertsen, and D. R. Reichman, Phys. Rev. B **88**, 045318 (2013).

[6] G. Berghäuser and E. Malic, Phys. Rev. B **89**, 125309 (2014).

[7] T. Olsen, S. Latini, F. Rasmussen, and K. S. Thygesen, Phys. Rev. Lett. **116**, 056401 (2016).

[8] A. Chernikov, T. C. Berkelbach, H. M. Hill, A. Rigosi, Y. Li, O. B. Aslan, D. R. Reichman, M. S. Hybertsen, and T. F. Heinz, Phys. Rev. Lett. **113**, 076802 (2014).

[9] D. Y. Qiu, F. H. da Jornada, and S. G. Louie, Phys. Rev. Lett. **111**, 216805 (2013).

[10] T. C. Berkelbach, M. S. Hybertsen, and D. R. Reichman, Phys. Rev. B **92**, 085413 (2015).

[11] P. Gong, H. Yu, Y. Wang, and W. Yao, Phys. Rev. B **95**, 125420 (2017).

[12] T. Cao, M. Wu, and S. G. Louie, arXiv:1708.02227 [Phys. Rev. Lett. (to be published) (2018)].

[13] A. Srivastava and A. Imamoğlu, Phys. Rev. Lett. **115**, 166802 (2015).

[14] J. Zhou, W.-Y. Shan, W. Yao, and D. Xiao, Phys. Rev. Lett. **115**, 166803 (2015).

[15] A. Raja, A. Chaves, J. Yu, G. Arefe, H. M. Hill, A. F. Rigosi, T. Korn, C. Nuckolls, J. Hone, T. C. Berkelbach, P. Nagler, C. Schu, L. E. Brus, T. F. Heinz, D. R. Reichman, and A. Chernikov, Nat. Commun. **8**, 15251 (2017).

[16] L. Hedin, Phys. Rev. **139**, A796 (1965).

[17] M. S. Hybertsen and S. G. Louie, Phys. Rev. Lett. **55**, 1418 (1985).

[18] H.-P. Komsa and A. V. Krasheninnikov, Phys. Rev. B **86**, 241201 (2012).

[19] F. Hüser, T. Olsen, and K. S. Thygesen, Phys. Rev. B **88**, 245309 (2013).

[20] D. Y. Qiu, F. H. da Jornada, and S. G. Louie, Phys. Rev. B **93**, 235435 (2016).

[21] Density functional theory calculations were performed with the Quantum ESPRESSO software package [43] with the Perdew-Burke-Ernzerhof exchange-correlation functional [44], norm-conserving pseudopotentials, and a $12 \times 12 \times 1$ ($12 \times 12 \times 3$) sampling of the Brillouin zone for the monolayer (bulk).

[22] N. S. Rytova, Vestn. Mosk. Univ. Fiz. Astron. **3**, 30 (1967).

[23] L. Keldysh, JETP Lett. **29**, 658 (1979).

[24] P. Cudazzo, I. V. Tokatly, and A. Rubio, Phys. Rev. B **84**, 085406 (2011).

[25] M. Kumagai and T. Takagahara, Phys. Rev. B **40**, 12359 (1989).

[26] K. Andersen, S. Latini, and K. S. Thygesen, Nano Lett. **15**, 4616 (2015).

[27] K. T. Winther and K. S. Thygesen, 2D Mater. **4**, 025059 (2017).

[28] L. E. Brus, J. Chem. Phys. **79**, 5566 (1983).

[29] D. Xiao, G.-B. Liu, W. Feng, X. Xu, and W. Yao, Phys. Rev. Lett. **108**, 196802 (2012).

[30] J. B. Neaton, M. S. Hybertsen, and S. G. Louie, Phys. Rev. Lett. **97**, 216405 (2006).

[31] In reality, the screening of bulk TMDCs is anisotropic, and one could imagine using a more complicated but realistic reference potential; however, using a coarse-grained treatment of the anisotropy $W^{ref}(\boldsymbol{r},\boldsymbol{r}') = e^2/[\varepsilon_z \varepsilon_{xy} \rho^2 + \varepsilon_{xy}^2 (z - z')^2]^{1/2}$ gives the same result in the order $z \to z'$ with $\rho = 0$.

[32] B. L. Evans and P. A. Young, Proc.-R. Soc. Edinburgh, Sect. A: Math. Phys. Sci. **284**, 402 (1965).

[33] M. Ugeda, A. Bradley, S. Shi, and H. Felipe, Nature Mater. **13**, 1091 (2014).

[34] J. Ryou, Y.-S. Kim, S. KC, and K. Cho, Sci. Rep. **6**, 29184 (2016).

[35] Y. Li, A. Chernikov, X. Zhang, A. Rigosi, H. M. Hill, A. M. van der Zande, D. A. Chenet, E.-M. Shih, J. Hone, and T. F. Heinz, Phys. Rev. B **90**, 205422 (2014).

[36] A. Steinhoff, M. Rösner, F. Jahnke, T. O. Wehling, and C. Gies, Nano Lett. **14**, 3743 (2014).

[37] D. Y. Qiu, F. H. Da Jornada, and S. G. Louie, Nano Lett. **17**, 4706 (2017).

[38] N. Peimyoo, W. Yang, J. Shang, X. Shen, Y. Wang, and T. Yu, ACS Nano **8**, 11320 (2014).

[39] M. Feierabend, G. Berghäuser, A. Knorr, and E. Malic, Nat. Commun. **8**, 14776 (2017).

[40] K. S. Novoselov, A. Mischenko, A. Carvalho, and A. H. C. Neto, Science **353**, aac9439 (2016).

[41] Z. Lin, A. McCreary, N. Briggs, S. Subramanian, K. Zhang, Y. Sun, X. Li, N. J. Borys, H. Yuan, S. K. Fullerton-Shirley, A. Chernikov, H. Zhao, S. McDonnell, A. M. Lindenberg, K. Xiao, B. J. LeRoy, M. Drndic, J. C. M. Hwang, J. Park, M. Chhowalla, R. E. Schaak, A. Javey, M. C. Hersam, J. Robinson, and M. Terrones, 2D Mater. **3**, 042001 (2016).

[42] N. R. Wilson, P. V. Nguyen, K. Seyler, P. Rivera, A. J. Marsden, Z. P. Laker, G. C. Constantinescu, V. Kandyba, A. Barinov, N. D. Hine, X. Xu, and D. H. Cobden, Sci. Adv. **3**, e1601832 (2017).

[43] P. Giannozzi, S. Baroni, N. Bonini, M. Calandra, R. Car, C. Cavazzoni, D. Ceresoli, G. L. Chiarotti, M. Cococcioni, I. Dabo, A. D. Corso, S. Fabris, G. Fratesi, S. de Gironcoli, R. Gebauer, U. Gerstmann, C. Gougoussis, A. Kokalj, M. Lazzeri, L. Martin-Samos, N. Marzari, F. Mauri, R. Mazzarello, S. Paolini, A. Pasquarello, L. Paulatto, C. Sbraccia, S. Scandolo, G. Sclauzero, A. P. Seitsonen, A. Smogunov, P. Umari, and R. M. Wentzcovitch, J. Phys.: Condens. Matter **21**, 395502 (2009).

[44] J. P. Perdew, K. Burke, and M. Ernzerhof, Phys. Rev. Lett. **77**, 3865 (1996).